 doi:10.20944/preprints202008.0717.v1

Article

Microvesicle formation induced by oxidative stress in human erythrocytes

Julia Sudnitsyna[1†], Elisaveta Skverchinskaya[2†], Irina Dobrylko[2], Elena R. Nikitina[2], Stepan Gambaryan[2], Igor Mindukshev [2,*]

[1] Center for Theoretical Problems of Physico-Chemical Pharmacology, Russian academy of sciences, Kosygina st., 4, Moscow, Russia, 119991; julia.sudnitsyna@gmail.com (J.S.);
[2] Sechenov Institute of Evolutionary Physiology and Biochemistry, Russian academy of sciences, Thorez pr., 44, Saint-Petersburg, Russia, 194223; lisarafail@mail.ru (E.S.); dobrylko@mail.ru (I.D.); elena.nikitina@bk.ru (E.R.N.); s.gambaryan@klin-biochem.uni-wuerzburg.de (S.G.); iv_mindukshev@mail.ru (I.M.);
[*] Correspondence: iv_mindukshev@mail.ru; Tel.: +7-921-979-4793
[†] These authors contributed equally to this work.

Abstract: Extracellular vesicles (EVs) released by different cell types play significant role in many physiological and pathophysiological processes. In physiological conditions red blood cells (RBCs) derived EVs compose 4 - 8% of all circulating EVs, and oxidative stress (OS) as a consequence of different pathophysiological conditions significantly increases the amount of circulated RBC-derived EVs, however the mechanisms of EV formation are not fully defined yet. To analyze OS-induced EV formation and RBCs transformations we used flow cytometry to evaluate cell esterase activity, caspase-3 activity, and band 3 clustering. Band 3 clustering was additionally analyzed by confocal microscopy. Two original laser diffraction-based approaches were used for analysis of cell deformability and band 3 activity. Hemoglobin species were characterized spectrophotometrically. We showed that cell viability in *tert*-butyl hydroperoxide-induced OS directly correlated with oxidant concentration to cell count ratio, RBCs-derived EVs contained hemoglobin oxidized to hemichrome (HbChr). OS induced caspase-3 activation and band 3 clustering in cells and EVs. Importantly, we showed that OS-induced EV formation is independent from calcium. Presented data indicated that during OS RBCs eliminate HbChr by vesiculation, in order to sacrifice the cell itself thereby prolonging lifespan and delaying the untimely clearance of in all other respects healthy RBCs.

Keywords: erythrocytes; microparticles; oxidative stress; vesiculation; band 3; t-BOOH, NO-donor; A23187

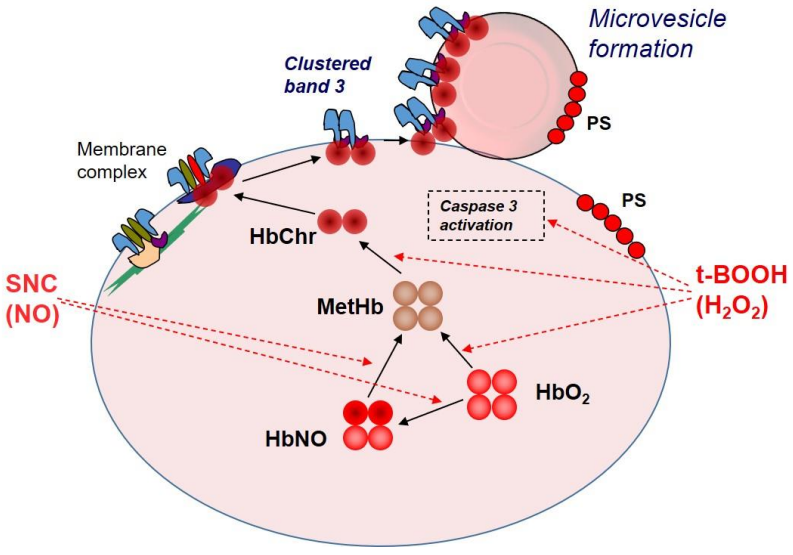

 doi:10.20944/preprints202008.0717.v1

Figure for Graphical abstract. Proposed mechanisms of oxidative stress-induced microvesicles formation in erythrocytes. Strong oxidative stress induced by t-BOOH (H2O2) oxidize hemoglobin to MetHb with subsequent oxidation to hemichrome (HbChr). HbChr binds to Band 3 protein and lead to its clustering and formation of microvesicles containing oxidized hemoglobin and PS at their surface. SNC (NO) oxidize Hb only to MetHb without future oxidation to HbChr and microvesicles formation.

1. Introduction

Extracellular vesicles (EVs) which consist of microvesicles (MVs), microparticles (MPs), and exosomes, are continuously produced in human blood from different cell types including circulating and endothelial cells. EVs contain various molecules of parent cells such as different proteins, bioactive lipids, and RNAs which could be taken up by recipient cells [1]. EVs are directly involved in different physiological processes like vasoregulation, thrombosis, hemostasis, inflammation etc., acting similarly to signaling molecules or by direct transport of their constituents [2, 3]. In normal conditions red blood cells (RBCs)-derived EVs compose 4 -8% of all circulating EVs [4]. EV formation is triggered by structural alterations of cell membrane which are driven by factors that disrupt erythrocyte skeleton-membrane attachment, including aging-associated oxidative damage [5, 6], reactive oxygen species (ROS) [7], increased intracellular Ca^{2+} concentration [8, 9], ATP depletion [10], and RBCs storage in blood banks [11]. RBCs-derived EVs are not homogeneous by their size and content. Increase of intracellular calcium concentration induces membrane shedding which produces EVs containing cytoskeleton proteins, glycophorin, band 3 protein (band 3, AE1), acetylcholine esterase, but not hemoglobin (Hb) [12]. During RBC concentrates storage EVs carry aggregates of Hb, band 3, cytoskeleton proteins, caspase 3 and 8, CD47 and IgGs [13]. Throughout the 120 days RBCs life span up to 20% of Hb is lost due to EV formation [14]. Formation of such EVs is proposed to rescue RBCs by getting rid of damaged Hb molecules and clustered band 3, which are well-defined markers of senescent RBCs, therefore prolonging the life span of these cells [15]. Two major mechanisms are described for EV formation including increase of intracellular calcium concentration and oxidative stress (OS)-induced Hb oxidation [16]. Ca^{2+}-activated protease calpain is involved in vesiculation by binding and degrading band 3, band 4.1 and ankyrin which lead to alteration of cell deformability [9, 16-19]. OS triggers membrane and Hb oxidation, clustering and disruption of band 3 - cytoskeleton anchorage, and all these alterations lead to EV formation [17, 20-24]. All these data indicate that there are various mechanisms of RBCs-derived EV formation, however several questions are still unsolved. In this study we elucidated the effects of different stimuli such as oxidant concentration, Hb oxidation state, role of calcium, caspase-3 activation, band 3 clustering that trigger RBCs EV formation.

Here we showed that cell viability in tert-butyl hydroperoxide-induced OS was directly correlated with ratio of oxidant concentration to cell count, RBCs-derived EVs contained Hb oxidized to hemichrome (HbChr). OS induced caspase-3 activation and clustering of band 3 protein in cells and EVs. Importantly, we showed that OS-induced EV formation was independent from calcium. Presented data indicated that during OS RBCs eliminate HbChr by vesiculation, in order to sacrifice the cell itself thereby prolonging lifespan and delaying the untimely clearance of in all other respects healthy RBCs.

2. Materials and Methods

2.1 Reagents and Chemicals

Calcein-AM and Eosin-5-Maleimide (EMA) were from Molecular probes (Eugene, USA). Annexin-V-FITC was obtained from Biolegend (Amsterdam, Netherlands). Anti-Active Caspase-3 FITC polyclonal antibody were from BD Pharmingen (San Diego, USA). Tert-butyl hydroperoxide (t-BOOH), S-nitroso-L-cysteine (SNC): sodium nitrite and L-cysteine hydrochloride monohydrate, calcium ionophore A23187 and basic buffer constituents were from Sigma–Aldrich (Munich,

Germany). The buffers were isotonic with osmolality 300 mOsm/kg H_2O controlled by cryoscopic osmometer Osmomat 3000 (Gonotec, Germany), pH 7.4, and had the following composition (in mM): HEPES-buffer (Buffer 1) - NaCl, 140; KCl, 5; HEPES, 10; $MgCl_2$, 2; *D*-glucose, 5; Ammonia-buffer (Buffer 2) - NH_4Cl, 140; KCl, 5; HEPES, 10; $MgCl_2$, 2; *D*-glucose, 5. Ca^{2+} (2mM) or EGTA (2mM) were added to Buffer 1 as indicated.

2.2 Methods

2.2.1 RBCs preparation. Citrated human blood was obtained from healthy volunteers, who did not take any medication at least 10 days before the experiments, after they gave informed consent. Blood draw was performed according to our institutional guidelines and the Declaration of Helsinki. Studies using human RBCs were approved by the local ethics committee of the Sechenov Institute of Evolutionary Physiology and Biochemistry RAS (Study No.3-03; 02.03.2019). RBCs were prepared by centrifugation of citrated whole blood at 400g (Centrifuge ELMI-50CM, Elmi, Latvia) in Buffer 1 with EGTA for 3 minutes at room temperature. Washed RBCs were resuspended in Buffer 1 with EGTA or Ca^{2+} as indicated and adjusted to $0.5x10^9$ cells/mL (corresponding to Hematocrit 4.0 – 4.5%). The main blood parameters (red blood cell count and mean cell volume – MCV) were controlled by the hematological counter Medonic-M20 (Boule Medical A.B., Sweden).

2.2.2 Stress models. Oxidative stress was induced by *tert*-Butyl hydroperoxide, t-BOOH (0.25, 0.5, 1, 1.5, 2mM). Calcium stress, as increased intracellular Ca^{2+} concentration, was inducted by calcium ionophore A23187 (1μM). Nitrosative stress was inducted by S-nitroso-L-cysteine, SNC (500μM).

2.2.3 Microparticle isolation and analysis. In this study we investigated EVs and divided them by their size, as characterized by flow cytometry, and content, as characterized by spectrophotometry, to MPs, which are smaller in size and did not contain Hb, and MVs, which were bigger in size and contained Hb. MPs/MVs isolation was performed according the protocol described in detail in [25]. Briefly, for analysis of MPs/MVs RBCs were incubated with the indicated compounds for 24 h, then the samples were gently centrifuged (50g, 7min) and the supernatant was collected for the future analysis. RBCs supernatant was centrifuged at 20 000g for 30min (centrifuge 5810R, Eppendorf, Germany) for separation of free Hb and pellet containing MVs and MPs. The presence of MVs and MPs in pellet was confirmed by flow cytometry, and then MVs and MPs were scanned spectrophotometrically for Hb species analysis.

2.2.4 Spectral analysis of hemoglobin species. Absorption spectra of Hb species were registered by spectrophotometer SPECS SSP-715-M (Spectroscopic systems LTD, Moscow, Russia) in the wavelength range of 300 – 700 nm with a step size of 1 nm at 25°C. To study the effects of different stresses on free Hb, intact cells were hypoosmotically lyzed and then the indicated compounds were added, then the spectra were collected at indicated time. To study the Hb transformation in cells, RBCs were incubated with the indicated compounds for indicated time, then the cells were hypoosmotically lyzed and the free Hb spectra were scanned. To study the Hb species encapsulated in MPs/MVs, MPs/MVs were isolated as described in 2.2.3 and scanned.

Hemoglobin species calculation. The percentage of oxidized Hb in RBC suspensions was determined by spectrophotometry using the millimolar extinction coefficients of the different Hb species (oxyHb, metHb, HbChr) according to [26]. Briefly, RBC lysates were scanned from 500 to 700 nm while recording the absorbance values at 560, 577, 630, and 700 nm. These data were used for the calculation of Hb species % using the equations presented in [26]. The data are presented as % from the sum of all Hb in the sample taken as 100%.

Induction of hypoxia. RBCs suspension was degassed with argon for 15min. Oxygen sensor mini-Oksik 3 ("Analitika service" LTD) was used to control the oxygen content in hypoxia chamber (Billups-Rothenberg), absorption was registered in the range of 300 -700 nm. The cuvette was sealed up with wrapping film during the registration of absorption for hypoxic conditions maintenance.

2.2.5 Characterization of RBCs deformability by laser diffraction method.

To estimate the osmotic and ammonium fragility of RBCs novel laser diffraction method (laser microparticle analyzer LaSca-T, BioMedSystems, Russia), adapted for cell physiology, was used according to Mindukshev et al. [27, 28]. The intensity of scattered light was continuously detected by

Preprints (www.preprints.org) | NOT PEER-REVIEWED | Posted: 31 August 2020 doi:10.20944/preprints202008.0717.v1

forward scattering at various angles (Supplementary Figures A1, A2). The MCV data from hematological counter Medonic-M20 (Boule Medical A.B., Sweden) were used as initial volume values MCV_{300} for the calculation of the MCV changes by the original software of the laser particle analyzer LaSca-TM.

Osmotic fragility test (OFT). RBCs ($0.5x10^9$ cells/mL) were incubated at indicated concentrations of A23187, SNC, t-BOOH at indicated time. Then aliquots (10 µl) of each sample was resuspended in1 ml of Buffer 1 for osmotic fragility test. Hemolysis curves were registered for a range of osmolality from 210 to 70 mOsm/kg H_2O. For each osmolality step corresponding volume of water and RBCs were added to the sample to keep RBC concentration constant. Cell volume investigation algorithm was used for estimation of cell volume changes dynamics and % of hemolysis [27, 29, 30]. Following parameters were calculated from hemolysis curves, H50, an osmotic fragility variable that represents the saline concentration which induces 50% lysis; W, the distribution width; MCV_{120}, maximal mean cell volume during the OFT which is calculated from hemolysis curve based on MCV_{300}. MCV_{300}, mean cell volume was controlled by hematological analyzer. The basic principles of the method are described in Supplementary Figure A1.

Ammonium stress test (AST). RBCs were prepared as for OFT. For control RBCs (10^6 cells/ml) were suspended in 1 ml of Buffer 1 with EGTA and then for AST in 1 mL of Buffer 2. Following parameters were calculated from the hemolysis curves, V_{hem}, maximal hemolysis rate; %Hem, % of lyzed cells; MCV_{hem}, maximal mean cell volume during the AST which is calculated from hemolysis curve based on MCV_{300}. The basic principles of the method are presented in Supplementary Figure A2.

2.2.6 Flow cytometry analysis

All flow cytometry experiments were performed on flow cytometer Navios (BeckmanCoulter, Brea, California, USA) with analysis of not less 20 000 events.

Size and structure analysis. For size and structure analysis FSC/SSC mode which provides information about cell size and structure was used. The intensity of light scattered in a forward direction (FSC) correlates with cell size. The intensity of scattered light measured at a right angle or side scatter (SSC) correlates with internal complexity, granularity and refractiveness [31-33].

Esterase activity analysis. Calcein-AM was used for the evaluation of cell esterase activity. RBCs (0.5×10^7 cells/mL) were incubated with Calcein-AM (5 µM, 40 min, 37°C) then diluted in 300µL buffer 1 with the following registration of Calcein fluorescence in FL1 by flow cytometer Navios (BeckmanCoulter, USA).

Phosphatidylserine externalization at the RBCs surface. Annexin-V is a Ca^{2+}-dependent dye, thus 2mM Ca^{2+} was added to Buffer 1 for Annexin test. RBCs ($0.5x10^9$ cells/mL) were incubated with Annexin-V (0.1µg/ml, 15min, 25°C), then fluorescence of Annexin was registered in FL1 by flow cytometry.

Analysis of band 3 clustering. The contribution of cytoskeleton in RBCs transformation under OS was estimated using eosin-5-maleimide (EMA) test. RBCs ($0.5x10^9$ cells/ml) were incubated with EMA in the Buffer 1 (0.07 mM, 40min) with the following EMA fluorescence intensity registration in FL1 by flow cytometry.

Microparticle detection. MPs and MVs were isolated as described in 2.2.3. The combined range of the cytometer optical system was used for data collection W2 (Wide-High 9◦ -19◦ + Narrow 2◦–9◦ mode). For W2 FSC detection, Ultra Rainbow Fluorescent Particles nominal size 3.0-3.4 µm (SPHERO™ Rainbow Fluorescent Particles Cat#URFP-30-2) and Latex Beads 0.5 µm (BeckmanCoulter, Cat# 7502468-BA) were used to estimate MP/MV sizes.

Caspase-3 activation. RBC $0.5x10^9$ cells/mL were incubated with indicated concentrations of A23187, SNC, t-BOOH at indicated time, fixed in 1% formalin (10 min), centrifuged (400g, 3min). Pellets then were resuspended in PBS BSA 1% and permeabilized by 1%Tween-20 for 10min. Anti-Active Caspase-3 FITC polyclonal antibodies were added to the samples and incubated for 20 min in the dark. Caspase-3 activity was registered as mean fluorescence intensity increase in FL1.

2.2.7 Confocal microscopy. Leica TCS SP5 MP scanning confocal microscope (Leica Microsystems Inc., Bannockburn, IL, USA) was used for evaluation of EMA-binding/band 3

 doi:10.20944/preprints202008.0717.v1

clustering and MPs and MVs formation. Erythrocytes were captured with 20 (HCX APO CS 20/0.70; Leica Microsystems, Inc.) or 63 (HCX APO CS 63/1.4; Leica Microsystems, Inc.) immersion objectives. To resolve fine details (clustering and MVs) an additional electronic zoom with a factor of 1.5 to 3.5 was used. For imaging the emitted fluorescence was acquired at 500 to 600 nm (green region of spectrum for EMA). Single focal plane images were merged and analyzed with standard Leica LAS AF Software (Leica Microsystems, Inc.)

2.2.8 Data analysis. Laser diffraction data were analyzed by the original software LaSca_32 v.1498 of the laser particle analyzer LaSca-TM. Flow cytometry data were analyzed by original software Cytometry List Mode Data Acquisition & Analysis Software for Navios cytometer 1.2 (BeckmanCoulter, USA) and by FCS Express Flow 7 (De Novo Software, CA, USA). Differences between groups were analyzed by IBM SPSS Statistics v.26 (IBM Corporation, Armonk, USA). The data are presented as the mean ± SD. Our variables conformed to a normal distribution (Shapiro-Wilk's test, $p > 0.05$). We used one-way analysis of variance (ANOVA) for group comparisons. When the samples were homoscedastic (Levene's test, $p > 0.05$) we used Tukey HSD post-hoc analysis. When the equal variances were not assumed, Tamhane's T2 post-hoc analysis was used. For paired groups analysis paired t-test was used. $P < 0.05$ was considered statistically significant.

Preprints (www.preprints.org) | NOT PEER-REVIEWED | Posted: 31 August 2020 doi:10.20944/preprints202008.0717.v1

3. Results

3.1 RBCs viability strongly depends on the ratio of oxidant to cell count

Calcein-AM could be used for evaluation of RBCs viability and OS induced cytotoxicity [34]. Therefore, in our experiments, we used this test to assess the effects of OS on RBCs viability through esterase activity changes. In constant RBCs concentration ($0.5x10^9$ cells/mL) Calcein fluorescence intensity significantly decreased with t-BOOH concentration increase (Figure 1A and B). Whereas, in constant t-BOOH concentration Calcein fluorescence intensity directly correlated with RBCs count (Figure 1C). Analysis of these two plots (Figures 1B and C) revealed exponential dependency ($R^2 = 0.98$) between Calcein fluorescence intensity, as a marker of OS, and ratio of oxidant concentration to cell count [t-BOOH]/RBC) (Figure 1D). Here we showed that it is very important to consider the ratio ([t-BOOH]/RBC) for characterization of OS effects on RBCs. Based on the presented data for all our experiments we kept RBCs concentration ($0.5x10^9$ cells/mL) constant.

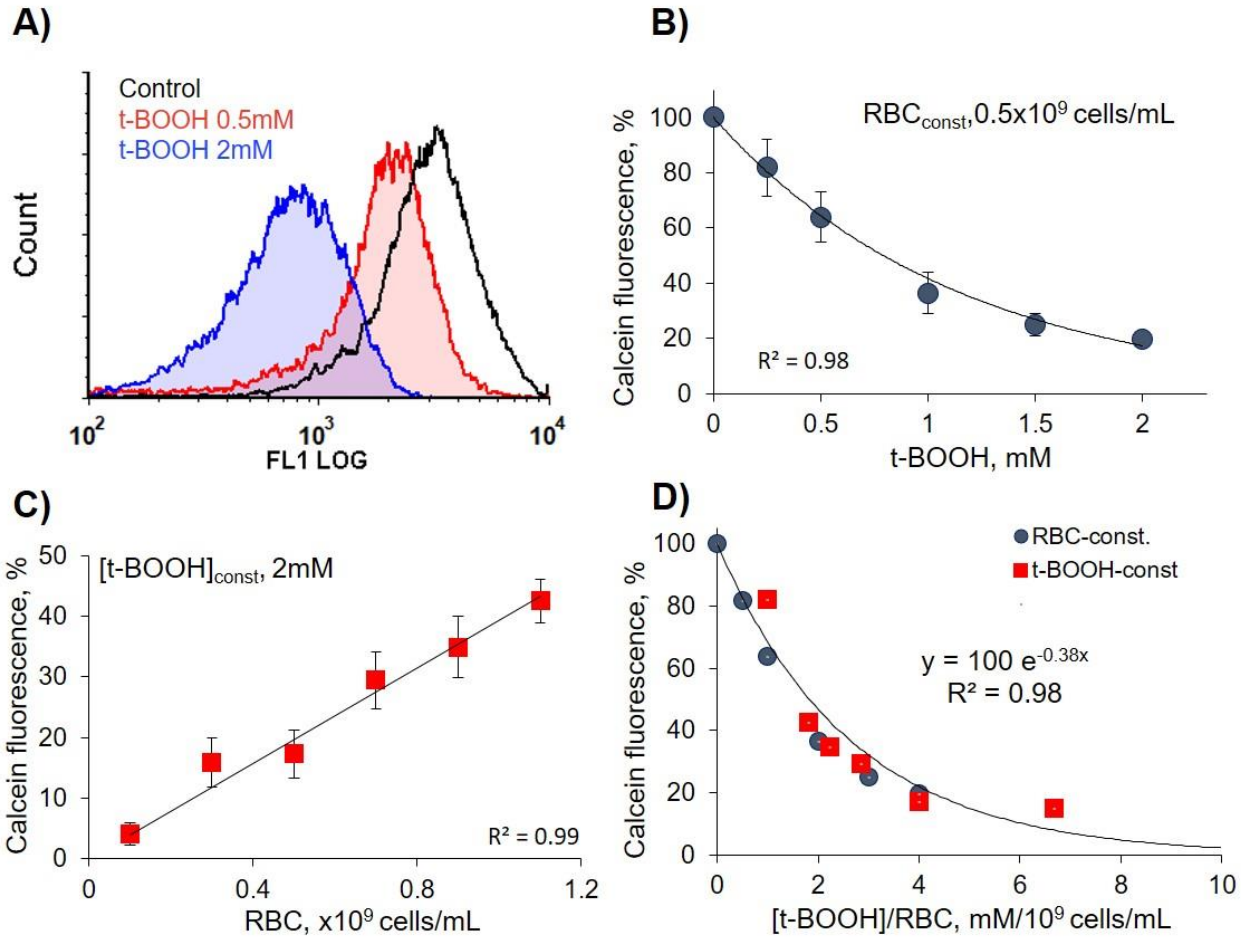

Figure 1. Calcein fluorescence intensity strongly depends on oxidant to cell count ratio. RBCs suspension was incubated with t-BOOH, at indicated concentrations for 1 hour, then RBCs were stained with Calcein-AM (5 μM, 40 min), and analyzed for Calcein fluorescence intensity by flow cytometry in FL1 (logarithmic scale). (**A)** representative histograms from 5 independent experiments. (**B)** dependence of Calcein fluorescence intensity in constant RBCs count from t-BOOH concentrations. (**C)** dependence of Calcein fluorescence intensity in constant t-BOOH concentration from RBCs count. (**D)** exponential dependency between Calcein fluorescence intensity and ratio of oxidant concentration/ cell count [t-BOOH]/RBC. Data in B, C are presented as Means ± SD, n = 5.

Preprints (www.preprints.org) | NOT PEER-REVIEWED | Posted: 31 August 2020 doi:10.20944/preprints202008.0717.v1

3.2 t-BOOH induces RBCs vesiculation

For analysis of RBCs transformations, we used flow cytometry protocol according to our previous template [29] and cell volume changes were analyzed by hematological analyzer (Figures 2, 3). For evaluation of different types of RBCs transformation dot plots were divided for four regions. Gate 1 represents the native cells, gate 2 - MPs, gate 3 – transformed cells with increased SSC values, gate 4 – MP with increased SSC values (referred to as microvesicles, MVs) (Figure 2).

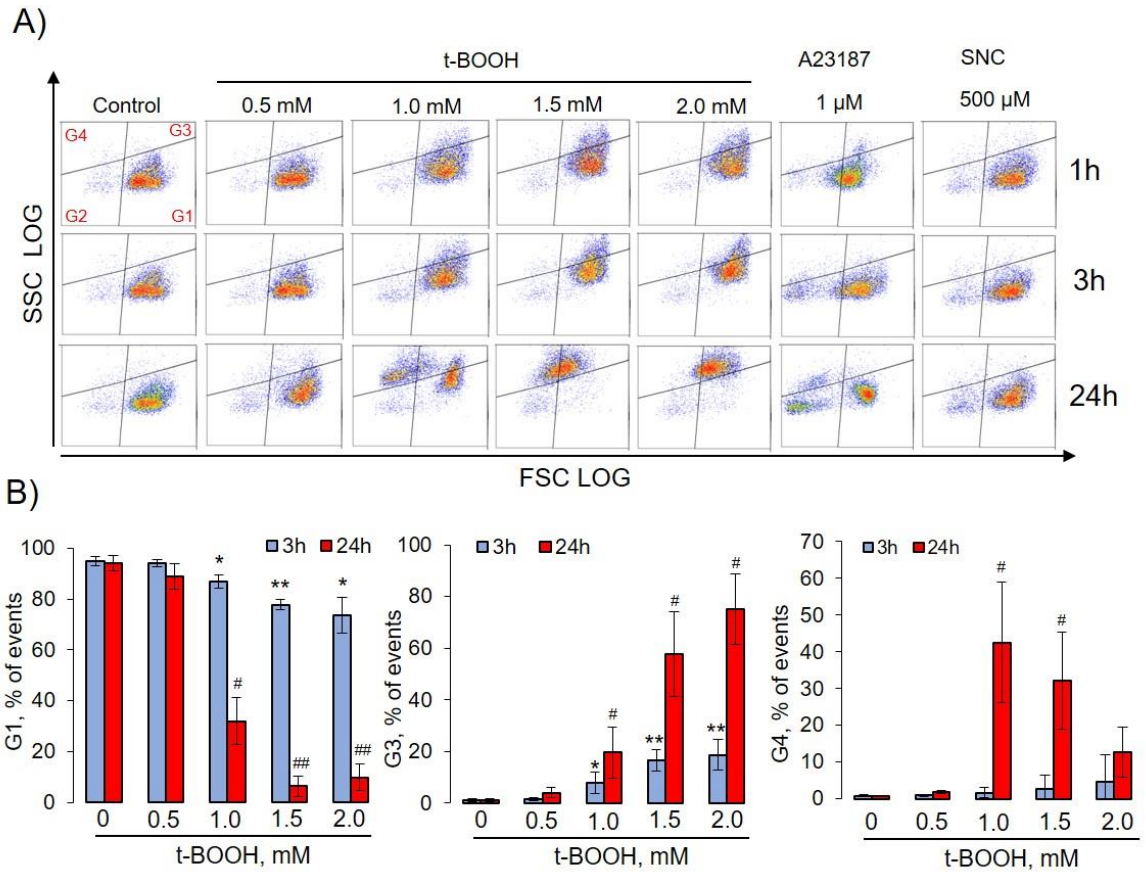

Figure 2. Oxidative stress induced by t-BOOH triggered RBCs transformation and microvesicle formation. RBCs ($0.5x10^9$ cells/mL) were incubated at indicated concentrations of t-BOOH, A23187, and SNC at indicated time. Gate 1 represents control RBCs, gate 2 MPs, gate 3 transformed RBCs, and gate 4 MVs. (**A)** Representative dot plots out of six independent experiments. **(B)** Quantification of presented data expressed as mean ± SD, n=6. One-way ANOVA, Tamhane T2 (G1, G2 24h, G4) or Tukey HSD post-hoc (G2 3h) were used where appropriate. *, $p < 0.05$, **, $p < 0.001$ compared to control (t-BOOH 0mM 3h); #, $p < 0.05$, ##, $p < 0.001$ compared to control (t-BOOH 0mM 24h).

In control more than 96% of RBCs are in gate 1and remain constant during 24 h. t-BOOH during 1- and 3-hour concentration dependently slightly increased FSC (cell volume) and increased SSC values (structural heterogeneity) without increase in MP formation. After 24 h of 0.5 mM of t-BOOH application cells slightly increased SSC and FSC values, whereas 1- and 1.5 mM led to formation of MVs and cells with increased SSC (gates 3, 4). 2 Mm of t-BOOH transformed RBCs to high SSC (gate 3). Increase of intracellular calcium concentration (A23187) time-dependently triggered MP formation (gate 2). Effects of SNC on RBCs during 1 – 24 h were similar to t-BOOH in concentration 0.5 mM. It is important to mention that t-BOOH induced only MV (gate 4), but not MP (gate 2) formation. Analysis of RBCs MCV changes is presented in Figure 3. Low doses of t-BOOH (0.5 – 1.5 mM) increased cell volume, whereas 2 mM of t-BOOH did not significantly change cell volume. In contrast A23187 significantly decreased MCV and SNC had no significant effects on MCV.

Preprints (www.preprints.org) | NOT PEER-REVIEWED | Posted: 31 August 2020 doi:10.20944/preprints202008.0717.v1

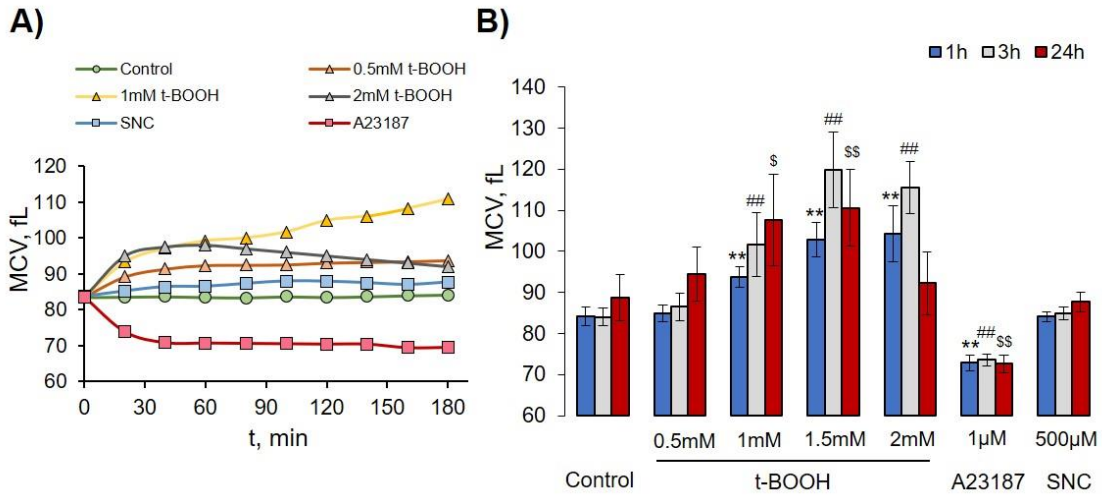

Figure 3. Effects of t-BOOH, A23187 and SNC on RBCs volume changes**.** RBCs ($0.5x10^9$ cells/mL) were incubated with indicated concentration of t-BOOH, A23187, and SNC for indicated time and analyzed by hematological analyzer. **(A)** representative histogram of MCV changes for one donor for 3 h, symbols indicate time of analysis. **(B)** Quantitative data from 10 independent experiments (10 donors). Data are presented as Mean ± SD (n = 10), one-way ANOVA, Leven's test < 0.05, Tamhane T2 post-hoc. *, $p < 0.05$, **, $p < 0.001$ compared to 1h control; #, $p < 0.05$, ##, $p < 0.001$ compared to 3h control; $, $p < 0.05$, $$, $p < 0.001$ compared to 24h control.

3.3 Oxidative stress induces hemoglobin oxidation to ferryl (hemichrome) forms

To maintain maximum oxygen-carrying capacity, Hb must be kept under reducing conditions in the ferrous (Fe^{2+}) formed by an efficient enzymatic machinery [35]. $HbFe^{2+}$, could spontaneously and during OS be oxidized to form $HbFe^{3+}$ (ferric Hb, methemoglobin, metHb), $HbFe^{4+}$ (ferryl Hb), and $\cdot HbFe^{4+}$ (ferryl radical). These oxidatively unstable Hb intermediates (ferryl/ferryl protein radicals refer to as hemichromes, HbChr) oxidize residues within the Hb globin chains (and other proteins within proximity), ultimately leading to Hb degradation and heme loss [36]. We used several compounds that can oxidase Hb and elucidated their effects on Hb oxidation state (Figure 4).

First, we tested the effects of used compounds on free Hb (Figures 4A and B), then intact cells were oxidized, lysed in hypoosmotic conditions and corresponding spectra were scanned (Figure 4C). t-BOOH firstly oxidized Hb to MetHb followed by oxidation to HbChr (Figure 4A). To evaluate the effects of NO donor (SNC) we used hypoxic conditions by application of N_2. SNC first formed HbNO then was oxidized to MetHb without significant formation of HbChr (Figures 4B, C, E, Table 1). MPs and MVs were collected from RBCs after 24h of application of indicated compounds and then supernatants and MV and MP containing pellets were scanned spectrophotometrically (Figure 4D). t-BOOH induced MVs contained ferryl forms of Hb, whereas SNC and A23187 produced MPs did not contain any significant amount of Hb. The % of Hb species was calculated according to [26] and presented in Figure 4E and Table 1.

Preprints (www.preprints.org) | NOT PEER-REVIEWED | Posted: 31 August 2020 doi:10.20944/preprints202008.0717.v1

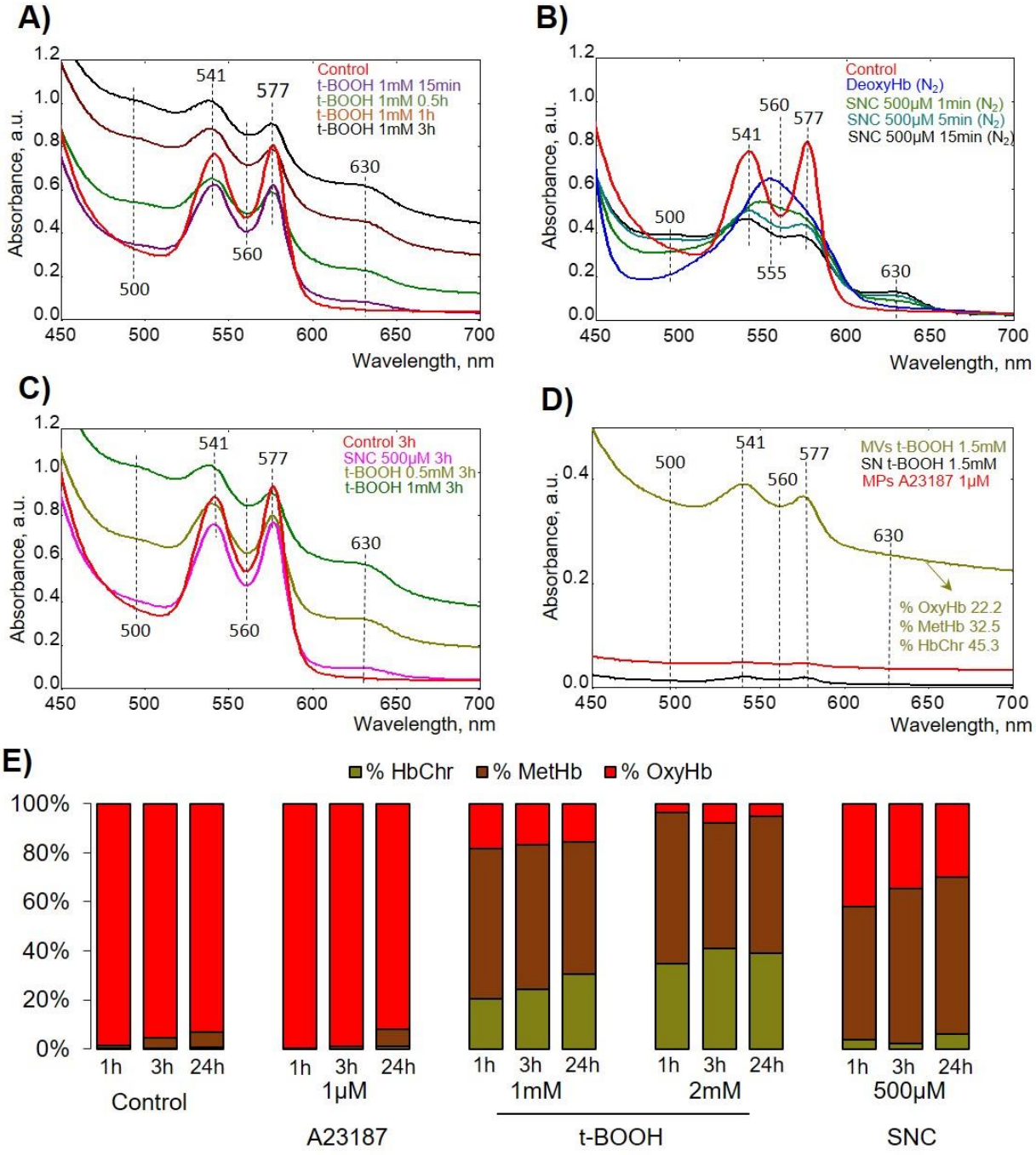

Figure 4. t-BOOH induces HbChr formation. Spectral scans from 450 to 700 nm captured the different oxidation states of Hb identified by characteristic peaks in the visible region. **(A)** Representative spectra of free Hb oxidation by 1mM t-BOOH (ferric, 500 and 630 nm; ferryl/HbChr, 545 nm, 576 nm, and a flattened region between 600 and 700 nm) in comparison with intact Hb spectra (ferrous, 541 and 576 nm) in Buffer 1 at 25°C in kinetics. **(B)** Representative spectra of free Hb oxidation by 500µM SNC in deoxygenated by N_2 Buffer 1 at 25°C in kinetics. Free oxyHb was deoxygenated by N_2 then SNC was added for indicated time. **(C)** Spectra of Hb from hypoosmotically lysed RBCs after 3 h treatment with indicated compounds at indicated concentrations. **(D)** After 24 h of RBCs incubation with indicated compounds, MVs and MPs were collected as described in Methods, then MVs/MPs and supernatant (SN) from last washing step were analyzed. (**E)** Representative bar chart of Hb species calculated from one donor.

Preprints (www.preprints.org) | NOT PEER-REVIEWED | Posted: 31 August 2020 doi:10.20944/preprints202008.0717.v1

Table 1. The % of Hb species formation in response to indicated compounds calculated according to Kanias et al. [26].

	Control		t-BOOH						A23187		SNC	
			0.5 mM		1mM		2mM		1µM		500µM	
	1h	3h	1h	3h	1h	3h	1h	3h	1h	3h	1h	3h
% OxyHb	98.0 ± 2.0	95.6 ± 3.0	66.3 ± 4.2 *	45.3 ± 3.9 *	30.7 ± 9.0 **	27.0 ± 13.6 **	20.9 ± 16.4 **	20.7 ± 15.1 **	97.4 ± 3.1	96.6 ± 3.0	47.2 ± 5.9 **	33.1 ± 3.4 **
%MetHb	1.8 ± 0.1	4.0 ± 2.3	30.6 ± 5.1 *	49.1 ± 6.6 *	50.5 ± 8.1 **	47.0 ± 11.8 **	58.8 ± 9.4 **	46.1 ± 6.6 **	2.3 ± 0.5	3.4 ± 0.6	50.8 ± 4.1 **	63.4 ± 4.6 **
% HbChr	0.2 ± 0.6	0.4 ± 0.2	4.9 ± 3.6	5.4 ± 2.1	18.8 ± 5.4 *	25.9 ± 8.1 **	20.3 ± 12.8 *	33.2 ± 9.1 **	0.3 ± 0.2	0.2 ± 0.1	2.5 ± 1.4	3.6 ± 2.5

Data are presented as means ± SD (n = 7), one-way ANOVA, Leven's test < 0.05, Tamhane T2 post-hoc.

*, $p<0.05$, **, $p<0.001$, compared to corresponding control (1h or 3h).

Preprints (www.preprints.org) | NOT PEER-REVIEWED | Posted: 31 August 2020 doi:10.20944/preprints202008.0717.v1

3.4 t-BOOH dose-dependently decreases RBCs deformability

The osmotic fragility of RBCs is a composite index of their shape, hydration, and, within certain limitations, proneness to in vivo destruction [37, 38]. In standard OFT the percent of hemolysis in increasingly hypotonic solution (0.75%, 0.65%, and 0.60%) is recorded spectrally by optical density. We developed the original automated, easy method for analysis of cells osmotic fragility. Previously for analysis of band 3 function we established the original ammonium stress-test based on band 3-RhAG facilitated ability of RBCs to swell and lyse in isoosmotic ammonium buffer (Buffer 2) [28]. To characterize OS-induced RBCs transformations in conditions favorable for MVs and MPs release we used these two tests. The basic principles of these tests are described in methods (2.2.5) and in Supplementary Figures A1 and A2.

1 h t-BOOH (0.5 – 1 mM) treatment led to increase of H_{50} (the osmolality that triggers hemolysis of 50% cells), indicating the elevated fragility, and high doses (2 mM) decreased H_{50}, indicating the increased rigidity (Figure 5A) in comparison with the control cells. OS dose-dependently increased cell distribution width (W). Both parameters strongly indicated the significant decrease in RBCs deformability and increase in RBCs heterogeneity.

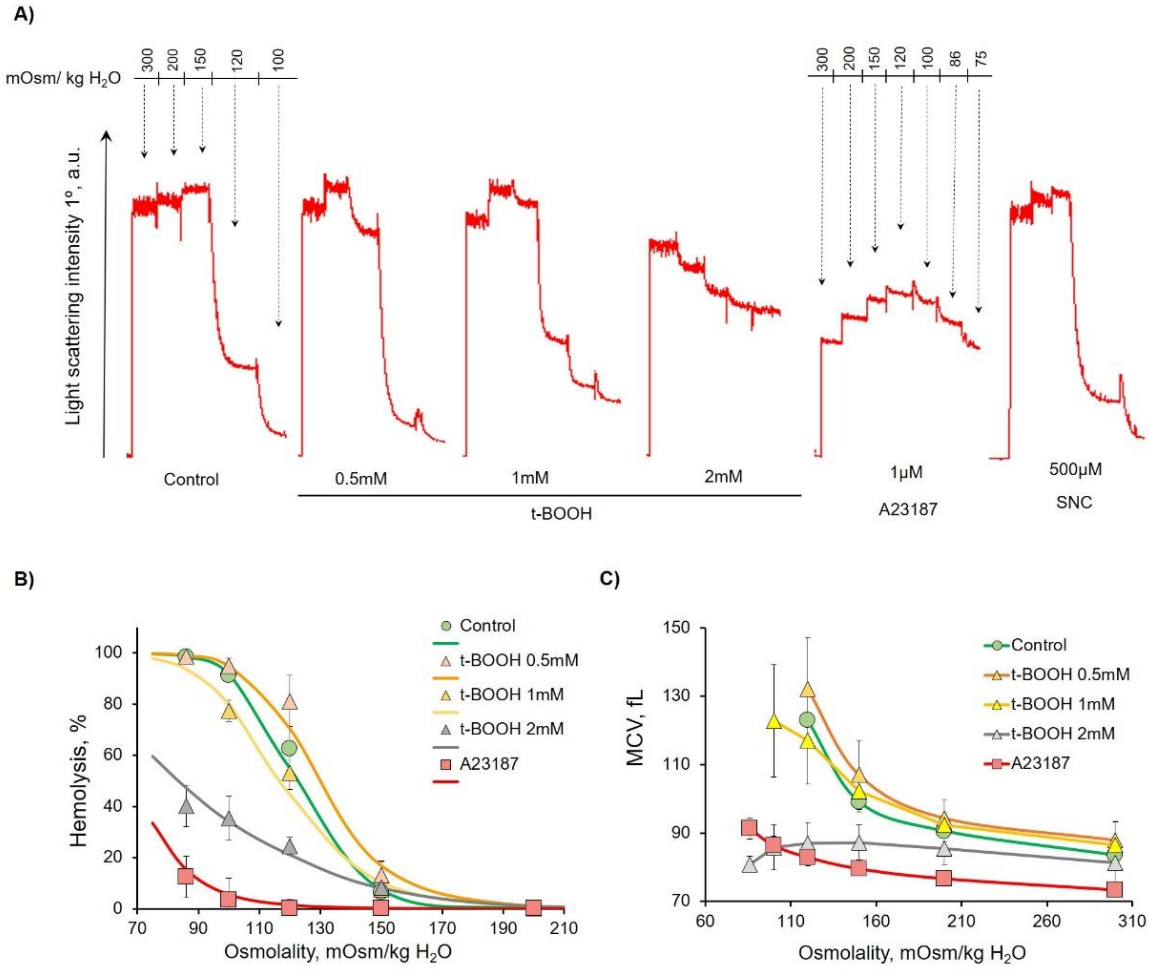

Figure 5. OS induced decrease in osmotic fragility of RBCs. RBCs ($0.5x10^9$ cells/mL) were incubated with the indicated substances during 1h, then aliquots (10μL, 10^6 cells/mL final concentration) of samples were resuspended in Buffer 1 with EGTA to register light scattering intensity corresponding to control. Then the osmolality was gradually reduced by H2O supplementation from 300 to 70 mOsm/kg H2O, to maintain the RBCs concentration, the corresponding number of cells was added at each step of H2O supplementation. (A) Representative osmotic hemolysis curves from OFT; (B) Quantification of % of hemolysis from osmotic fragility test calculated from 6 independent

 doi:10.20944/preprints202008.0717.v1

experiments; (C) Quantification of MCV during osmotic fragility test calculated from 6 independent experiments.

After 1h of treatment A23187 led to significant decrease of MCV_{300} and subsequent MCV_{120}, and significant decrease of H_{50} indicating the decreased deformability. SNC effects were similar to 0.5mM of t-BOOH, MCV_{300} and MCV_{120}, W and H_{50} were slightly increased in comparison to control cells. The osmotic fragility test parameters are summarized in Table 2.

Table 2. Quantification of osmotic fragility test data of 6 independent experiments (donors).

	Control	t-BOOH			A23187	SNC
		0.5mM	1mM	2mM	1 μM	500 μM
H_{50}, mOsm/kg H_2O	122 ± 9	130 ± 7	117 ± 8	83 ± 6**	68 ±7**	128 ± 6
W, mOsm/kg H_2O	44 ± 7	52 ± 8	60 ± 9*	107 ± 10**	41 ± 6	47 ± 7
MCV_{300}, fL	84 ± 2	88 ± 6	87 ± 7	81 ± 6	73 ± 2**	86 ± 5
MCV_{120}, fL	124 ± 9	131 ± 8	115 ± 8	88 ± 6*	83 ± 2**	127 ± 4

MCV_{300} – data from hematology cell counter. Data are presented as means ± SD (n = 6), one-way ANOVA, if Leven's test < 0.05, Tamhane T2 post-hoc (MCV_{300},), if Leven's test > 0.05, Tukey HCD post-hoc (H_{50}, W, MCV_{120}). *, $p<0.05$, **, $p<0.001$, compared to corresponding control.

Ammonium stress-test results after 1h were similar to osmotic fragility test (Figure 6). %Hem (% of hemolyzed cells), V_{hem} (hemolysis maximal rate), and MCV_{hem} (maximal mean cell volume during the ammonium stress test) as the markers of rigidity dose-dependently significantly decreased with the rise in t-BOOH concentration, indicating the increased RBCs rigidity and inhibited band 3 protein activity.

Preprints (www.preprints.org) | NOT PEER-REVIEWED | Posted: 31 August 2020 doi:10.20944/preprints202008.0717.v1

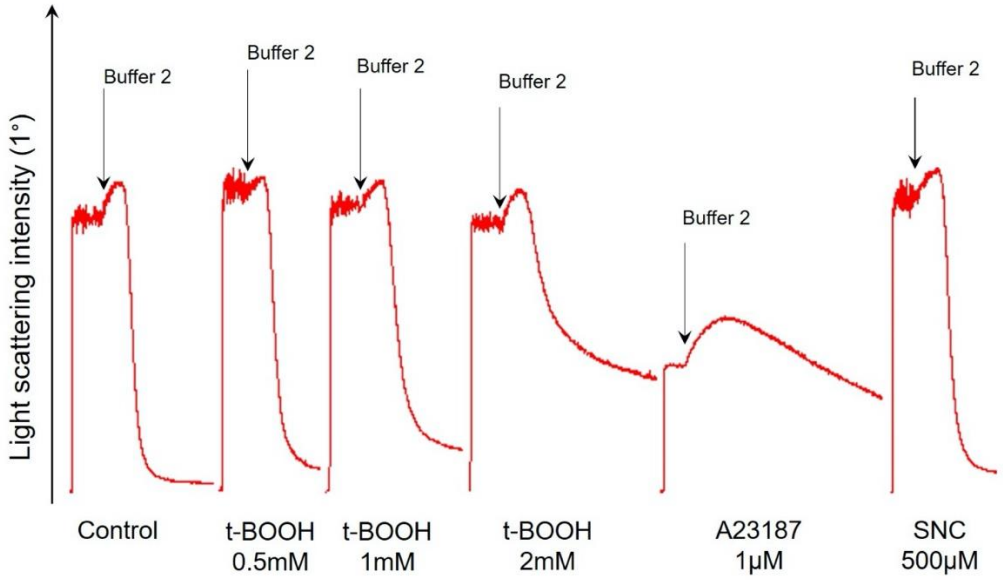

Figure 6. OS dose-dependently decreased RBCs deformability and inhibited band 3 function. Representative hemolysis curves of ammonium stress test one of 8 experiments. RBCs ($0.5x10^9$ cells/mL) were incubated with the indicated compounds during 1h, then aliquots (10 µL, 10^6 cells/mL final concentration) of samples were resuspended in Buffer 1 to register light scattering intensity corresponding to control. Then aliquots (10 µL, 10^6 cells/mL final concentration) of samples were resuspended in Buffer 2 for ammonium stress-test. Arrows indicate the start of ammonium stress test. Quantitation of these data is presented in Table 3.

As described [39, 40] increase in intracellular calcium concentration significantly altered RBCs deformability. In our experiments, RBCs treatment with A23187 led to significant decrease in all the tested parameters. SNC effects were similar to 0.5mM of t-BOOH, all the parameters did not significantly differ compared to control. Quantification of ammonium stress test data are presented in Table 3.

Table 3. Quantification of ammonium stress test data of 5 independent experiments (donors).

	Control	t-BOOH				A23187	SNC
		0.5mM	1mM	1.5mM	2mM	1 µM	500 µM
V_{hem}	1.00±0.02	1.01±0.02	0.71±0.21	0.57±0.08*	0.32±0.09*	0.06±0.02**	1.04±0.02
% Hem	96.5±0.2	92.1±2.6	80.8±11.4	69.3±9.6*	47.8±13.2**	40.0±11.3**	95.6±1.0
MCV_{300}	84.9±0.9	86.7±2.3	87.5±5.9	87.8±4.3	88.6±10.4	70.5±3.7*	86.87±1.9
MCV_{hem}	142.3±3.2	143.8±4.8	124.5±9.8	116.0±1.7*	105.1±1.9**	96.3±6.5**	141.0±2.8

MCV_{300} – data from hematology cell counter; Data are presented as means ± SD (n=5), one-way ANOVA, if Leven's test < 0.05, Tamhane T2 post-hoc (V_{hem}, MCV_{300}, MCV_{120}), if Leven's test > 0.05, Tukey HSD post-hoc (%Hem). *, $p<0.05$, **, $p<0.001$, compared to corresponding control.

Preprints (www.preprints.org) | NOT PEER-REVIEWED | Posted: 31 August 2020 doi:10.20944/preprints202008.0717.v1

3.5 OS induced RBCs transformation and microvesicle formation is independent on extracellular calcium concentration

Calcium plays significant role in RBCs function [41-43] and triggers eryptosis [44], however the role of calcium in MV formation is not clear yet. Therefore, we compared MV formation, PS surface exposure, and caspase 3 activation in RBCs during OS induced by different t-BOOH concentrations, A23187, and SNC, in Buffer 1 with calcium or with EGTA (Figures 7 - 9). For MV formation analysis we used the same template as in 3.2 and calculated events in gates G1, G3 and G4 in HEPES-buffer containing calcium (2 mM) or EGTA (2 mM). Surprisingly, calcium had no significant effect on OS-induced RBCs transformation and MV formation (Figure 7A - D). Next, we tested whether PS surface exposure (Annexin-V binding) as a marker of eryptosis is dependent on extracellular calcium. Similar to MV formation, calcium had no significant effect on OS-induced Annexin V binding (Figure 8A-B). We compared % of Annexin V positive cells after A23187, t-BOOH and SNC treatment (Figure 8C). A23187 and t-BOOH after 3 h significantly increased PS exposure, whereas SNC had no significant effect.

In different conditions PS surface exposure might be dependent, or independent on caspase-3 activation [45, 46]. t-BOOH induced strong caspase-3 activation (Figure 9A and B) which, like MV formation and PS surface exposure was independent on calcium. In all tested conditions A23187 and SNC did not significantly activate caspase-3 (Figure 9B).

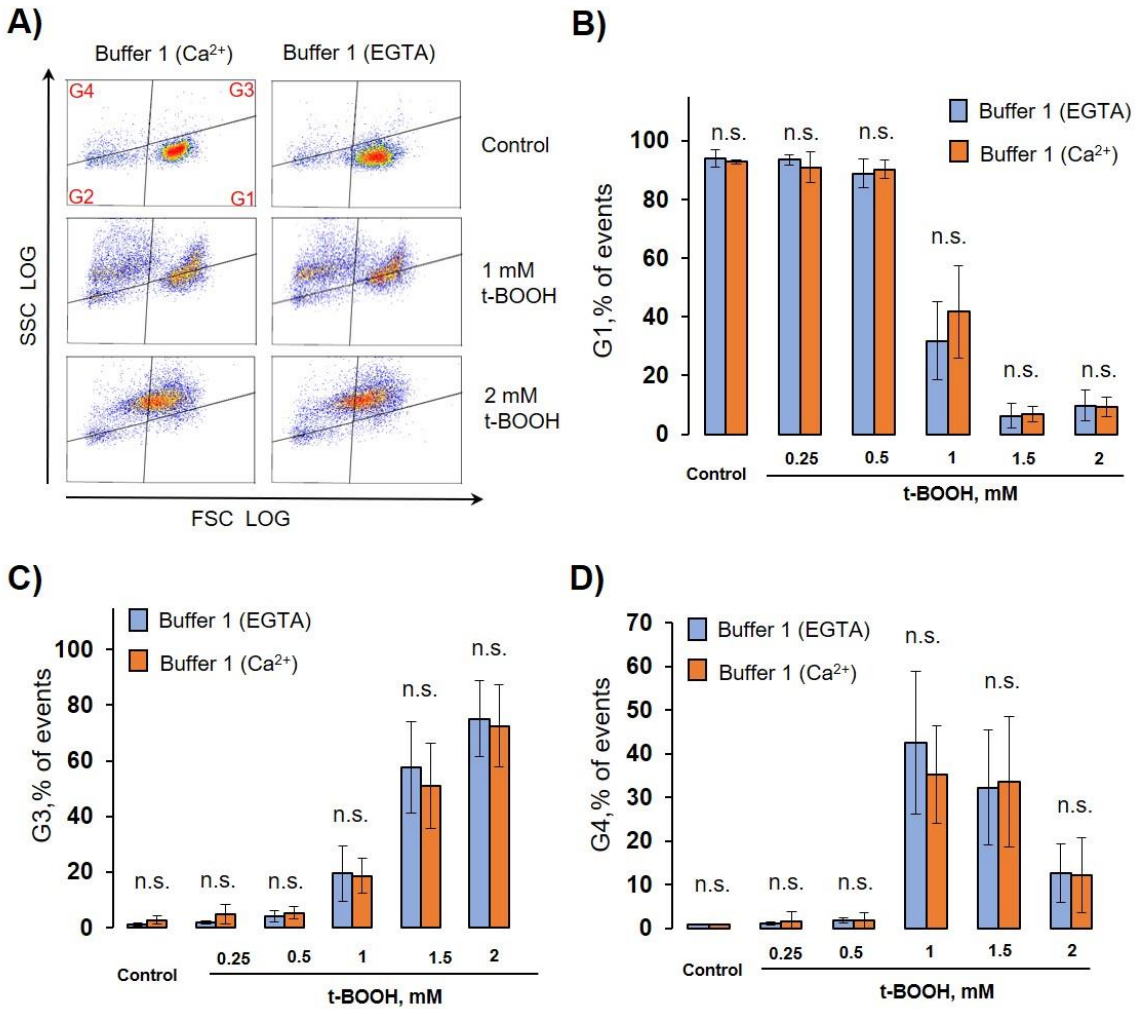

Figure 7. OS-induced RBCs transformation and MV formation are calcium independent. RBCs (0.5x10^{9}cells/mL) were incubated with indicated concentration of t-BOOH in Buffer 1 containing 2 mM calcium, or 2 mM EGTA, for indicated time and analyzed by flow cytometry. **(A)** Representative SSC/FSC dot plots of one out of six independent experiments for 24 h. Template and gating

Preprints (www.preprints.org) | NOT PEER-REVIEWED | Posted: 31 August 2020 doi:10.20944/preprints202008.0717.v1

correspond to 3.2. **(B-D)** Calculation of events distributed in the corresponding gates. Data are presented as Mean ± SD (n = 7), paired t-test; n.s., not significant.

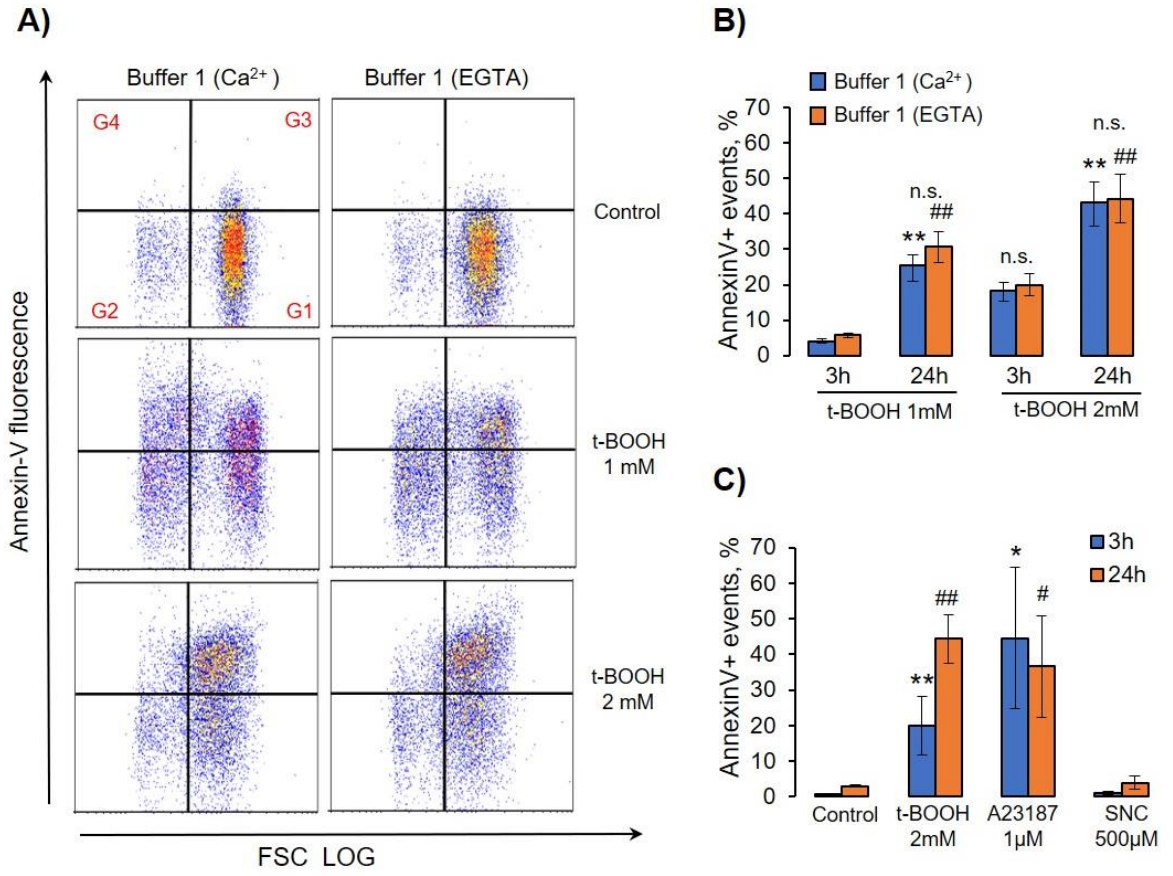

Figure 8. OS-induced Annexin-V binding is calcium independent. RBCs ($0.5x10^9$ cells/mL) were incubated with indicated concentrations of t-BOOH, A23187, and SNC in buffer 1 containing 2 mM Ca^{2+}, or 2 mM EGTA for indicated time. Annexin-V (0.1μg/ml, 15min, 25°C) was added to treated cells and analyzed by flow cytometry. **(A)** Representative Annexin V/FSC dot plots of one out of six independent experiments for 24 h. Gate G1 corresponds to control cells; G2, Annexin-V negative EVs; G3, Annexin-V positive cells; G4, Annexin-V positive EVs. **(B, C)** Calculation of Annexin-V positive events in G3 and 4. Data on B-D are presented as the mean ± SD, in (B) – paired t-test, **, $p < 0.001$, compared to 3h in Buffer 1 with Ca^{2+}; ##, $p < 0.001$, compared to 3h in Buffer 1 with EGTA; n.s. – not significant. In (C) – one-way ANOVA, Levens's test < 0.05, Tamhane's T2 post-hoc, *, $p < 0.05$, **, $p < 0.001$ compared to 3h control; #, $p < 0.05$, ##, $p < 0.001$ compared to 24h control;

Preprints (www.preprints.org) | NOT PEER-REVIEWED | Posted: 31 August 2020 doi:10.20944/preprints202008.0717.v1

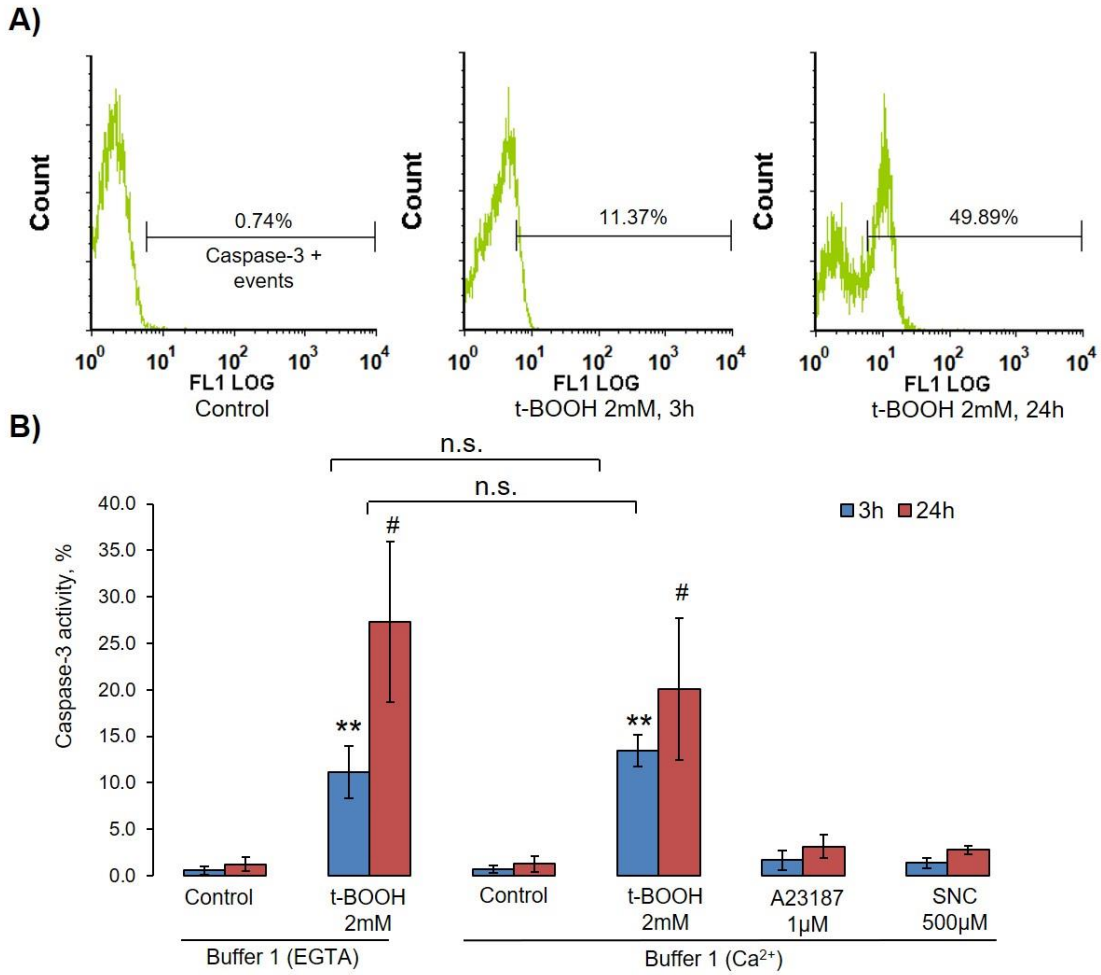

Figure 9. t-BOOH-induced OS activated caspase 3 in RBCs. RBCs (0.5x10^9 cells/mL) were incubated with indicated concentrations of t-BOOH, A23187, and SNC in Buffer 1 containing 2 mM calcium, or 2 mM EGTA for indicated time. After incubation with indicated compounds cells were fixed by 1% (final concentration) of methanol-free formaldehyde, permeabilized by 0.5% Tween for 20 min, then anti-active caspase-3 antibodies were added for 30 min and caspase-3 activation was measured by flow cytometry according to manufacturer instructions. **(A)** Original histograms from one of seven independent experiments; **(B)** Data quantification based on seven independent experiments. Data are presented as the mean ± SD (n=7), one-way ANOVA (Buffer 1 with EGTA both 3h and 24h), Tukey HSD post-hoc (Buffer 1 with Ca^{2+} 3h), Tamhane T2 post-hoc (Buffer 1 with Ca^{2+} 24h); paired t-test Buffer 1 (EGTA) and Buffer 1 (Ca^{2+}), ** $p < 0.001$ compared to corresponding control, # $p < 0.05$ compared to corresponding control, n.s. – not significant.

3.6 t-BOOH-induced OS triggers band 3 clustering

Oxidative stress induces band 3 oxidation and dissociation from spectrin skeleton, resulting in enhanced mobility and subsequent band 3 clusters formation [21, 24, 47]. In our experiments we tested whether each of used compound triggers band 3 clustering by applying EMA binding test. As expected, in control cells EMA showed slight homogeneous fluorescence (Figure 10A). During t-BOOH -induced OS in both RBCs and RBCs-derived MV clustering of band 3 was detected (Figure 10A). In contrast, A23187 and SNC did not induce neither MV formation nor band 3 clustering (Figure 10C) and, as expected, A23187 triggered echinocytosis in RBC (Figure 10A).

Preprints (www.preprints.org) | NOT PEER-REVIEWED | Posted: 31 August 2020 doi:10.20944/preprints202008.0717.v1

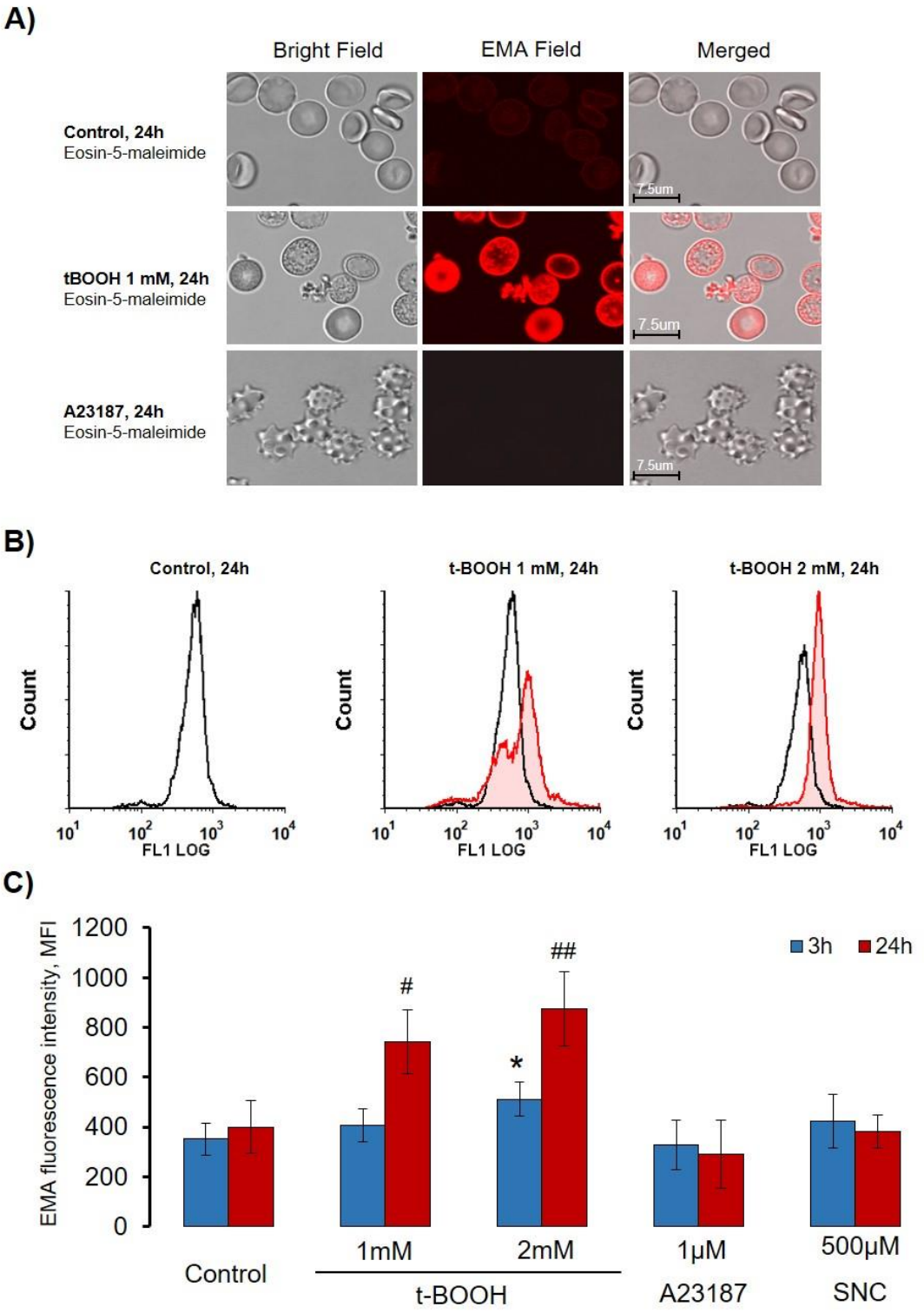

Figure 10. t-BOOH induced oxidative stress led to band 3 clustering and MVs formation. RBCs ($0.5x10^9$ cells/mL) were incubated as indicated with t-BOOH, A23187 and SNC at indicated time, followed by EMA staining (0.07mM, 40min). **(A)** representative confocal images of t-BOOH transformed RBCs. RBCs were processed for confocal microscopic analysis as described in the method part (2.2.7). **(B)** original histograms of EMA fluorescence intensity after 24h t-BOOH treatment. **(C)** Quantification of flow cytometry data. Data are presented as Mean ± SD (n = 7), one-way ANOVA, Leven's test > 0.05, Tukey HSD post-hoc (3h), *, $p < 0.05$, compared to 3h control; Leven's test < 0.05, Tamhane T2 post-hoc (24h), #, $p < 0.05$, ##, $p < 0.001$ compared to 24h control.

 doi:10.20944/preprints202008.0717.v1

4. Discussion

Extracellular vesicles (EVs) released by different cell types play significant role in many physiological and pathophysiological processes. The cargo and types of EVs and their functional role are strongly dependent on the cell of origin and mechanisms of EV formation [48]. Two main mechanisms of RBCs derived EV formation connected with increase of intracellular calcium concentration and Hb oxidation were proposed [49]. Increase of intracellular calcium concentration leads to programmed cell death, so called eryptosis for RBCs [50], which could be triggered by numerous xenobiotics and exogenous substances [51] as well as several pathological states including diabetes, hepatic failure, sepsis, chronic kidney disease [52-56]. MPs formed during eryptosis by membrane shedding are around 200 nm in diameter and characterized by surface PS exposure [9]. However, the question whether EV formation during eryptosis is connected with classical apoptotic pathways (caspase-3 activation) is still under debates [7, 13]. In our experiments increase of intracellular calcium by application of A23187 led to strong PS surface exposure in both RBCs and EVs but did not activate caspase-3 (Figure 9B). In contrast, OS triggered PS exposure and EV formation was independent from calcium and activated caspase-3, which indicated that two different mechanisms, calcium-dependent, and independent, are responsible for surface PS exposure and EV formation. Classification of RBCs-derived EVs is also not clearly defined. Some authors referred to as microvesicles [13, 17] while others for the same kind of EVs used term microparticles [2, 3] without detailed characterization of differences between them. In our study we divided RBCs-derived EVs into two populations: a) EV derived from A23187 treated RBCs which are smaller in size and did not contain Hb are referred to as MPs, and b) OS-triggered EV, which were bigger in size and contained oxidized Hb are referred to as MVs [22]. Various compounds and pathological states definitely might trigger both pathways of RBCs-derived EV formation, however in our study we focused mainly on important conditions which facilitate OS-induced RBCs transformation, MV formation, and characterization of these MVs.

Increase of intracellular calcium concentration is regarded as the main driving force of RBCs transformation and EV formation [17] OS-induced increase of intracellular calcium mobilization was shown in several publications [41, 57], however the question whether it is the main trigger of RBC transformation remains open, therefore in our experiments, we first tested influence of extracellular calcium on RBC transformation and EV formation comparing Buffer 1 with 2 mM calcium or with 2 mM EGTA (calcium free buffer). Surprisingly, we found no significant differences in OS-induced RBCs transformation and EVs formation in these two conditions. Most of our experiments were done in Buffer 1 with 2 mM EGTA (EGTA-containing buffer), similar experiments were performed in the Buffer 1 with 2 mM calcium (Figure 7) and there were no significant differences in RBCs transformation, Annexin-V binding (Figures 8 A,B), MV formation, or caspase-3 activation (Figure 9B). Based on these data we concluded that most likely Hb oxidation to HbChr but not increase of intracellular calcium concentration is the main driving force of OS-induced RBCs transformation and EV formation.

Next important question raised in our study was connected with oxidant and RBCs concentration, and time of incubation with oxidant (Figure 1). In most of the literature t-BOOH is used to induce OS in RBCs with highly controversial results, from increase of cell volume to cell shrinkage, size, content of produced microparticles and cell deformability. Here we showed that RBCs transformation, deformability, band 3 clustering, and MV formation in t-BOOH-induced OS strongly depended on oxidant concentration/time and ratio of oxidant to cell count (Figure 1). t-BOOH concentration less than 0.5 mM did not induce significant changes in RBCs, MV formation started at concentrations 1 - 1.5 mM, whereas at 2 mM cells rigidity increased with reduced MV formation (Figure 5).

Another aspect of OS-induced RBCs transformation which was also an important part of our work and should be considered in future studies was connected with Calcein-AM test, a marker of cellular esterase activity. Clearly, esterase activity did not directly correlate with RBCs transformation and MV formation (Figures 1 and 2). t-BOOH dose-dependently reduced Calcein fluorescence,

however cells transformation and MV formation continued even in the conditions of almost completely inactivated esterase activity after 3 h of incubation with t-BOOH (Figure 2).

Such processes as senescence, hyperthermia, transfusion, increase of intracellular calcium concentration, RBCs storage in blood banks and oxidative stress accelerate RBCs vesiculation [11]. Through MV generation erythrocytes were shown to remove membrane patches containing removal molecules, damaged cell constituents and damaged membrane constituents [15, 17, 49]. In our experiments only t-BOOH induced formation of high SSC MVs which contained highly oxidized Hb (HbChr), whereas A23187 and SNC did not, indicating that RBC derived EVs were heterogeneous in content, with, or without Hb. These data indicated that during OS RBCs eliminate HbChr by vesiculation, in order to sacrifice the cell itself thereby prolonging lifespan and delaying the untimely clearance of in all other respects healthy RBCs.

5. Conclusions

OS-triggered RBCs transformation and MV formation is mediated by complex processes including Hb oxidation, band 3 clustering, cytoskeleton reorganization, increase of intracellular calcium concentrations and other alterations in RBCs cellular organization. OS could be developed as consequences of several pathological states like diabetes, sepsis, chronic kidney disease, hepatic failure, and the degree of OS and RBCs transformation might be significantly variable dependent on the conditions. t-BOOH is often used for analysis of RBCs in OS conditions, however published data are of RBCs reaction to OS are highly variable and dependent on concentration/time of t-BOOH administration. Therefore, we first established standards for evaluation of t-BOOH-induced OS and show that it is especially important to consider not only oxidant concentration, but the ratio of oxidant to cell count. Next, we developed two new original methods, ammonium and osmotic fragility tests, based on laser diffraction analysis of RBCs transformation, which allow to characterize RBCs osmotic and ammonium fragility. Thus, presented data, methodology, and new methods for analysis of OS-induced RBCs transformations will allow to characterize these cells more broadly during OS.

Supplementary Materials: The following are available online at www.mdpi.com/xxx/s1, Supplementary Figure A1: Evaluation of RBCs osmotic fragility by laser diffraction method; Supplementary Figure A2: Basic principles of ammonium stress-test.

Author Contributions: Conceptualization, I.M., J.S., and E.S.; methodology, I.M., E.S.; software, J.S., E.S.; validation, E.S., I.D. and E.R.N.; formal analysis, J.S.; investigation, E.S. and J.S.; resources, I.M.; data curation, I.M.; writing—original draft preparation, E.S., J.S., I.M.; writing—review and editing, S.G., J.S.; visualization, I.M., J.S. and E.S.; supervision, S.G.; project administration, J.S. and I.M.; funding acquisition, J.S. All authors have read and agreed to the published version of the manuscript.

Funding: This research was funded by the Russian Fund for Basic Researches (grant no.19-315-60015 to J.S.) and by the State Assignment of Ministry of Science and Higher Education of the Russian Federation (project no. AAAA-A18-118012290371-3 to E.S., I.D., E.R.N., S.G. and I.M.).

Acknowledgments: The authors would like to thank Sechenov Institute of Evolutionary Physiology and Biochemistry Core Facilities Center for providing the opportunity to use Navios cytometer.

Conflicts of Interest: The authors declare no conflict of interest. The funders had no role in the design of the study; in the collection, analyses, or interpretation of data; in the writing of the manuscript, or in the decision to publish the results.

References

1. Rosa-Fernandes, L.; Rocha, V.B.; Carregari, V.C.; Urbani, A.; Palmisano, G. A. Perspective on Extracellular Vesicles Proteomics. *Front Chem*. **2017**. *5*. 102. DOI: 10.3389/fchem.2017.00102.
2. Alexandru, N.; Costa, A.; Constantin, A.; Cochior, D.; Georgescu, A. Microparticles: From Biogenesis to Biomarkers and Diagnostic Tools in Cardiovascular Disease. *Curr Stem Cell Res Ther*. **2017**. *12*. 89–102. DOI: 10.2174/1574888X11666151203224058.

3. Said, A.S.; Rogers, S.C.; Doctor, A. Physiologic Impact of Circulating RBC Microparticles upon Blood-Vascular Interactions. *Front Physiol*. **2018**. 8. 1120. DOI:10.3389/fphys.2017.01120.
4. Shah, M.D.; Bergeron, A.L.; Dong, J.F.; López, J.A. Flow cytometric measurement of microparticles: pitfalls and protocol modifications. *Platelets*. **2008**. *19*. 365–372. DOI: 10.1080/09537100802054107.
5. Hattangadi, S.M.; Lodish, H.F. Regulation of erythrocyte lifespan: do reactive oxygen species set the clock? *J Clin Invest*. **2007**. *117*. 2075–2077. DOI:10.1172/JCI32559.
6. Bosman, G.J.; Lasonder, E.; Luten, M.; Roerdinkholder-Stoelwinder, B.; Novotný, V.M.; Bos, H.; De Grip, W.J. The proteome of red cell membranes and vesicles during storage in blood bank conditions. *Transfusion*. **2008**. *48*. 827–835. DOI:10.1111/j.1537-2995.2007.01630.x.
7. Mohanty, J.G.; Nagababu, E.; Rifkind, J.M. Red blood cell oxidative stress impairs oxygen delivery and induces red blood cell aging. *Front Physiol*. **2014**. *5*. 84. DOI:10.3389/fphys.2014.00084.
8. Bratosin, D.; Estaquier, J.; Petit, F.; Arnoult, D.; Quatannens, B.; Tissier, J.P.; Slomianny, C.; Sartiaux, C.; Alonso, C.; Huart, J.J.; Montreuil, J.; Ameisen, J.C. Programmed cell death in mature erythrocytes: a model for investigating death effector pathways operating in the absence of mitochondria. *Cell Death Differ*. **2001**. 8. 1143–1156. DOI: 10.1038/sj.cdd.4400946.
9. Nguyen, D.B.; Ly, T.B.; Wesseling, M.C.; Hittinger, M.; Torge, A.; Devitt, A.; Perrie, I.; Bernhardt, I. Characterization of Microvesicles Released from Human Red Blood Cells. *Cell Physiol Biochem.* **2016**. *38*. 1085–1099. DOI:10.1159/000443059.
10. Lutz, H.U.; Liu, S.C.; Palek, J. Release of spectrin-free vesicles from human erythrocytes during ATP depletion. I. Characterization of spectrin-free vesicles. *J Cell Biol*. **1977**. *73*. 548–560. DOI:10.1083/jcb.73.3.548.
11. D'Alessandro, A.; Kriebardis, A.G.; Rinalducci, S.; Antonelou, M.H.; Hansen, K.C.; Papassideri, I.S.; Zolla, L. An update on red blood cell storage lesions, as gleaned through biochemistry and omics technologies. *Transfusion*. **2015**. *55*. 205–219. DOI:10.1111/trf.12804.
12. Greenwalt, T.J. The how and why of exocytic vesicles. *Transfusion*. **2006**. *46*. 143-152. DOI: 10.1111/j.1537-2995.2006.00692.x.
13. Kriebardis, A.G.; Antonelou, M.H.; Stamoulis, K.E.; Economou-Petersen, E.; Margaritis, L.H.; Papassideri, I.S. RBC-derived vesicles during storage: ultrastructure, protein composition, oxidation, and signaling components. *Transfusion*. **2008**. *48*. 1943–1953. DOI: 10.1111/j.1537-2995.2008.01794.x.
14. Willekens, F.L.A.; Roerdinkholder-Stoelwinder, B.; Groenen-Döpp, Y.A.M.; Bos, H.J.; Bosman, G.J.C.G.M., van den Bos, A.G.; Verkleij A.J.; Were, J.M. Hemoglobin loss from erythrocytes in vivo results from spleen-facilitated vesiculation. *Blood*. **2003**. *101*. 747–751. DOI: 10.1182/blood-2002-02-0500.
15. Willekens, F.L.; Were, J.M.; Groenen-Döpp, Y.A.; Roerdinkholder-Stoelwinder, B.; de Pauw, B.; Bosman, G.J. Erythrocyte vesiculation: a self-protective mechanism? *Br J Haematol*. **2008**. *141*. 549–556. DOI: 10.1111/j.1365-2141.2008.07055.x
16. Pollet, H.; Conrard, L.; Cloos, A.S.; Tyteca, D. Plasma Membrane Lipid Domains as Platforms for Vesicle Biogenesis and Shedding? *Biomolecules*. **2018**. *8*. 94. DOI: 10.3390/biom8030094.

17. Leal, J. K. F.; Adjobo-Hermans, M. J. W.; Bosman G. J. C. G. M. Red Blood Cell Homeostasis: Mechanisms and Effects of Microvesicle Generation in Health and Disease. *Front Physiol.* **2018.** *9*. 703. DOI:10.3389/fphys.2018.00703.
18. Kostova, E.B.; Beuger, B.M.; Klei, T.R.; Halonen, P.; Lieftink, C.; Beijersbergen, R.L.; van den Berg, T. K.; Van Bruggen, R. Identification of signalling cascades involved in red blood cell shrinkage and vesiculation. *Biosci Rep*. **2015**. *35*. e00187. DOI: 10.1042/BSR20150019.
19. Cloos, A-S.; Ghodsi, M.;, Stommen, A.; Vanderroost, J.; Dauguet, N.; Pollet, H.; D'Auria, L.; Mignolet, E.; Larondelle, Y.; Terrasi, R.; Muccioli, G.G.; Van Der Smissen, P.; Tyteca, D. Interplay Between Plasma Membrane Lipid Alteration, Oxidative Stress and Calcium-Based Mechanism for Extracellular Vesicle Biogenesis From Erythrocytes During Blood Storage. *Front Physiol*. **2020**. *11*. 712. DOI: 10.3389/fphys.2020.00712.
20. Rifkind, J. M.; Nagababu, E. Hemoglobin redox reactions and red blood cell aging. *Antioxid Redox Signal*. **2013**. *18.* 2274–2283. DOI: 10.1089/ars.2012.4867
21. Arashiki, N.; Kimata, N.; Manno, S.; Mohandas, N.; Takakuwa, Y. Membrane Peroxidation and Methemoglobin Formation Are Both Necessary for Band 3 Clustering: Mechanistic Insights into Human Erythrocyte Senescence. *Biochem*. **2013**. *52*. 5760–5769. DOI: 10.1021/bi400405p.
22. Ferru, E; Pantaleo, A.; Carta, F.; Mannu, F.; Khadjavi, A.; Gallo, V.; Ronzoni, L.; Graziadei, G.; Cappellini, M.D.; Turrini, F. Thalassemic erythrocytes release microparticles loaded with hemichromes by redox activation of p72Syk kinase. *Haematologica*. **2014**. *99*. 570–578. DOI: 10.3324/haematol.2013.084533.
23. Mohanty, J.G.; Nagababu, E.; Rifkind, J.M. Red blood cell oxidative stress impairs oxygen delivery and induces red blood cell aging. *Front Physiol*. **2014**. *5*. 84. DOI:10.3389/fphys.2014.00084.
24. Jana, S.; Strader, M.B.; Meng, F.; Hicks, W.; Kassa, T.; Tarandovskiy, I.; De Paoli, S.; Simak, J.; Heaven, M.R.; Belcher, J.D.; Vercellotti, G.M.; Alayash, A.I. Hemoglobin oxidation-dependent reactions promote interactions with band 3 and oxidative changes in sickle cell-derived microparticles. *JCI Insight*. **2018**. *3*. e120451. DOI: 10.1172/jci.insight.120451;
25. Dinkla, S.; Brock, R.; Joosten, I.; Bosman, G.J. Gateway to understanding microparticles: standardized isolation and identification of plasma membrane-derived vesicles. *Nanomedicine (Lond)*. **2013**. *8*. 1657-1668. DOI:10.2217/nnm.13.149.
26. Kanias, T.; Acker, J.P. Mechanism of hemoglobin-induced cellular injury in desiccated red blood cells. *Free Radic Biol Med*. **2010**. *49*. 539-547. DOI: 10.1016/j.freeradbiomed.2010.04.024.
27. Mindukshev, I.; Gambaryan, S.; Kehrer, L.; Schuetz, C.; Kobsar, A.;, Rukoyatkina, N.; Nikolaev V.O.; Krivchenko, A.; Watson, S.P.; Walter, U.; Geiger, J. Low angle light scattering analysis: a novel quantitative method for functional characterization of human and murine platelet receptors. *Clin Chem Lab Med*. **2012**. *50*. 1253–1262. DOI:10.1515/CCLM.2011.817.
28. Mindukshev, I.; Kudryavtsev, I.; Serebriakova, M.; Trulioff, A.; Gambaryan, S.; Sudnitsyna, J.; Khmelevskoy, D.; Voitenko, N.; Avdonin, P.; Jenkins, R.; Goncharov, N. Flow cytometry and light scattering technique in evaluation of nutraceuticals. In: *Nutraceuticals: Efficacy, Safety and Toxicity*; Editor Gupta R.C., Elsevier: Oxford UK, **2016**. 319–332. DOI: doi.org/10.1016/B978-0-12-802147-7.00024-3.
29. Mindukshev, I.V.; Sudnitsyna, J.S.; Skverchinskaya, E.A.; Andreyeva A.Yu.; Dobrylko, I.A.; Senchenkova, E. Yu.; Krivchenko, A.I.; Gambaryan, S.P. Erythrocytes' Reactions to Osmotic,

Ammonium, and Oxidative Stress Are Inhibited under Hypoxia. *Biochemistry (Moscow), Suppl. Series A: Membrane and Cell Biology*. **2019**. *13*. 352–364. DOI: 10.1134/S1990747819040081.

30. Sudnitsyna, J.S.; Skverchinskaya, E.A.; Dobrylko, I.A.; Nikitina, E.R.; Krivchenko, A.I.; Gambaryan, S.P.; Mindukshev, I.V. Human erythrocyte ammonium transport is mediated by functional interaction of ammonium (RhAG) and anion (AE1) transporters. *Biochemistry (Moscow), Suppl. Series A: Membrane and Cell Biology*. **2016**. *10*. 301–310. DOI: 10.1134/S1990747816040097.
31. Darzynkiewicz, Z.; Juan, G.; Li, X.; Gorczyca, W.; Murakami, T.; Traganos, F. Cytometry in cell necrobiology: analysis of apoptosis and accidental cell death (necrosis). *Cytometry*. **1997**. *27*. 1–20. DOI: 10.1002/(SICI)1097-0320(19970101)27:1<1::AID-CYTO2>3.0.CO;2-L
32. Luchetti C.G.; Solano M.E.; Sander V., et al. Effects of dehydroepiandrosterone on ovarian cystogenesis and immune function. *J Reprod Immunol*. **2004**. *64*. 59–74. DOI: 10.1016/j.jri.2004.04.002
33. Tzur, A.; Moore, J.K.; Jorgensen, P.; Shapiro, H.M.; Kirschner, M.W. Optimizing optical flow cytometry for cell volume-based sorting and analysis. *PLoS One*. **2011**. *6*. e16053. DOI: 10.1371/journal.pone.0016053.
34. Bratosin, D.; Mitrofan, L.; Palii, C.; Estaquier, J.; Montreuil, J. Novel fluorescence assay using calcein-AM for the determination of human erythrocyte viability and aging. *Cytometry A*. **2005**. *66*. 78–84. DOI:10.1002/cyto.a.20152.
35. Kassa, T.; Jana, S.; Meng, F.; Alayash, A.I. Differential heme release from various hemoglobin redox states and the upregulation of cellular heme oxygenase-1. *FEBS Open Bio*. **2016**. *6*. 876–884. DOI: 10.1002/2211-5463.12103.
36. Chintagari, N.R.; Jana, S.; Alayas, A.I. Oxidized Ferric and Ferryl Forms of Hemoglobin Trigger Mitochondrial Dysfunction and Injury in Alveolar Type I Cells. *Am J Respir Cell Mol Biol*. **2016**. *55*. 288–298. DOI: 10.1165/rcmb.2015-0197OC.
37. King, M.J.; Zanella, A. Hereditary red cell membrane disorders and laboratory diagnostic testing. *Int J Lab Hematol*. **2013**. *35*. 237–243. DOI: 10.1111/ijlh.12070.
38. Walski, T.; Chludzińska, L.; Komorowska, M.; Witkiewicz, W. Individual osmotic fragility distribution: a new parameter for determination of the osmotic properties of human red blood cells. *Biomed Res Int*. **2014**. *2014*. 162102. DOI: 10.1155/2014/162102.
39. Huisjes, R.; Bogdanova, A.; van Solinge, W.W.; Schiffelers, R.M.; Kaestner, L.; van Wijk, R. Squeezing for Life - Properties of Red Blood Cell Deformability. *Front Physiol*. **2018**. *9*. 656. DOI: 10.3389/fphys.2018.00656.
40. Cueff, A.; Seear, R.; Dyrda, A.; Bouyer, G.; Egée, S.; Esposito, A.; Skepper, J.; Tiffert, T. Effects of elevated intracellular calcium on the osmotic fragility of human red blood cells. *Cell Calcium*. **2010**. *47*. 29–36. DOI: 10.1016/j.ceca.2009.11.002.
41. Bogdanova, A.; Makhro, A.; Wang, J.; Lipp, P.; Kaestner, L. Calcium in red blood cells - a perilous balance. *Int. J. Mol. Sci*. **2013**. *14*. 9848–9872. DOI: 10.3390/ijms14059848.
42. Kuck, L.; Peart, J.N.; Simmonds, M.J. Calcium dynamically alters erythrocyte mechanical response to shear [published online ahead of print, 2020]. *Biochim Biophys Acta Mol Cell Res*. **2020**. *1867*. 118802. DOI: 10.1016/j.bbamcr.2020.118802.
43. Kuck, L.; Peart, J.N.; Simmonds, M.J. Active modulation of human erythrocyte mechanics. *Am J Physiol Cell Physiol*. **2020**. *319*. C250–C257. DOI: 10.1152/ajpcell.00210.2020.

44. Lang, P.A.; Kaiser, S.; Myssina, S.; Wieder, T.; Lang, F.; Huber, S.M. Role of Ca2+-activated K+ channels in human erythrocyte apoptosis. *Am J Physiol Cell Physiol*. **2003**. *285*. C1553–C1560. DOI: 10.1152/ajpcell.00186.2003.
45. Hierso, R.; Waltz, X.; Mora, P.; Romana, M.; Lemonne, N.; Connes P.; Hardy-Dessources M-D. Effects of oxidative stress on red blood cell rheology in sickle cell patients. *Br J Haematol*. **2014**. *166*. 601–606. DOI: 10.1111/bjh.12912.
46. Raducka-Jaszul, O.; Bogusławska, D.M.; Jędruchniewicz, N.; Sikorski, A.F. Role of Extrinsic Apoptotic Signaling Pathway during Definitive Erythropoiesis in Normal Patients and in Patients with β-Thalassemia. *Int J Mol Sci*. **2020.** *21*. 3325. DOI: 10.3390/ijms21093325.
47. Shimo, H.; Arjunan, S.N.; Machiyama, H., Nishino, T.; Suematsu, M.; Fujita, H.; Tomita, M.; Takahashi, K. Particle Simulation of Oxidation Induced Band 3 Clustering in Human Erythrocytes. *PLoS Comput Biol*. **2015**. *11*. e1004210. DOI: 10.1371/journal.pcbi.1004210.
48. Hafiane, A.; Daskalopoulou, S.S. Extracellular vesicles characteristics and emerging roles in atherosclerotic cardiovascular disease. *Metabolism*. **2018**. *85*. 213–222. DOI: 10.1016/j.metabol.2018.04.008.
49. Tissot, J.D.; Rubin, O.; Canellini, G. Analysis and clinical relevance of microparticles from red blood cells. *Curr. Opin. Hematol*. **2010**. *17*. 571–577. DOI: 10.1097/moh.0b013e32833ec217.
50. Lang, E.; Qadri, S.M.; Lang, F. Killing me softly - suicidal erythrocyte death. *Int J Biochem Cell Biol.* **2012**. *44*. 1236–1243. DOI: 10.1016/j.biocel.2012.04.019.
51. Föller, M.; Lang, F. Ion Transport in Eryptosis, the Suicidal Death of Erythrocytes. *Front Cell Dev Biol*. **2020**. *8*. 597. DOI: 10.3389/fcell.2020.00597.
52. Carelli-Alinovi, C.; Misiti, F. Erythrocytes as Potential Link between Diabetes and Alzheimer's Disease. *Front Aging Neurosci*. **2017**. 9. 276. DOI: 10.3389/fnagi.2017.00276.
53. Turpin, C.; Catan, A.; Guerin-Dubourg, A.; Debussche, X.; Bravo, S.B.; Álvarez, E.; Van Den Elsen, J.; Meilhac, O.; Rondeau, P.; Bourdon, E. Enhanced oxidative stress and damage in glycated erythrocytes. *PLoS One*. **2020**. *15*. e0235335. DOI: 10.1371/journal.pone.0235335.
54. Föller, M.; Huber, S.M.; Lang, F. Erythrocyte programmed cell death. *IUBMB Life*. **2008**. *60*. 661–668. DOI: 10.1002/iub.106.
55. Bateman, R.M.; Sharpe, M.D.; Singer, M.; Ellis, C.G. The Effect of Sepsis on the Erythrocyte. *Int J Mol Sci.* **2017.** *18*, 1932. DOI: 10.3390/ijms18091932.
56. Lang, F.; Bissinger, R.; Abed, M.; Artunc, F. Eryptosis - the neglected cause of anemia in end stage renal disease. *Kidney Blood Press Res.* **2017**. *42*. 749–760. DOI: 10.1159/000484215.
57. Petrou, T.; Olsen, H.L.; Thrasivoulou, C.; Masters, J.R.; Ashmore, J.F.; Ahmed, A. Intracellular Calcium Mobilization in Response to Ion Channel Regulators via a Calcium-Induced Calcium Release Mechanism. *J Pharmacol Exp Ther*. **2017**. *360*. 378–387. DOI: 10.1124/jpet.116.236695.